Surface & Coatings Technology 217 (2013) 70–75

Contents lists available at SciVerse ScienceDirect

Surface & Coatings Technology

journal homepage: www.elsevier.com/locate/surfcoat

Thermal shock behavior of nanostructured and microstructured thermal barrier coatings on a Fe-based alloy

Changhai Zhou [a,b], Qiuming Zhang [c], Yao Li [b,*]

[a] Postdoctoral Research State of Materials Science and Engineering, Harbin Institute of Technology, Harbin 150001, China
[b] Center for Composite Materials and Structures, Harbin Institute of Technology, Harbin, 150001, China
[c] School of Chemical Engineering and Technology, Harbin Institute of Technology, Harbin 150001, China

ARTICLE INFO

Article history:
Received 22 May 2012
Accepted in revised form 28 November 2012
Available online 6 December 2012

Keywords:
TBCs
Fe–Cr–Ni
Air plasma spray
Thermal shock

ABSTRACT

Thermal barrier coatings (TBCs) of nanostructured and microstructured yttria stabilized zirconia (YSZ) were deposited on a Fe-based alloy of GH2132 by air plasma spray. The thermal shock behavior of both coatings was investigated in a comparative aspect. Scanning electron microscopy (SEM) and high resolution digital camera were employed to examine the surface and cross-sectional morphologies of coatings before and after thermal shock. Results revealed that nanostructured TBCs was superior to the microstructured TBCs in thermal shock performance. In the case of microstructured TBCs, both the TBC and the bond coat were separated from the substrate. However, the failure of nanostructured TBCs showed that only local TBC spalled and the penetrating cracks widened.

1. Introduction

Thermal barrier coatings (TBCs) have been widely used in modern gas turbine engine to lower the metal surface temperature in combustor and turbine section hardware. Because of their lower thermal conductivity and better chemical stability, TBCs play an important role in insulating heat flux to metal substrate, allowing an increase in operating temperature. Extensive investigations and reviews have been reported on the microstructure, failure, promising materials and fabrication techniques of TBCs [1–7]. There are four primary constituents in a TBC system. They are (i) an outermost TBC itself, (ii) an intermediate bond coat, (iii) a thermally grown oxide layer and (iv) the superalloy substrate. Failures of the TBCs are chemical and thermomechanical, such as interdiffusion between bond coat and metallic substrate [8], ceramic sintering [9–11], increasing stress due to the thermally grown oxide and thermal expansion mismatch [1–3], and thermomechanical fatigue [12–14].

In the previous investigations, Ni-based alloys are usually used as the metallic substrate based on the application of aerospace and navigation fields. As important as Ni-based alloy, some lower cost Fe-based alloys, such as GH2132 (Fe–25Cr–15Ni), are widely used in the power plants. Because the thermal expansion coefficient between these Fe-based alloys and the conventional TBCs including TBC itself and bond coat are so much different that the application of conventional TBCs on these Fe-based alloys is not suitable. Recently, the nanostructured TBCs on Ni-based alloys have been fast developed due to their potential properties of better mechanical properties, chemical stability and excellent thermal shock resistance [15–17]. Therefore, the authors attempted to deposit nanostructured TBCs on a Fe-based alloy of GH2132 to explore the potential suitable application of TBCs on these Fe-based alloys with high expansion coefficient. The preparation and comparative thermal shock behavior of conventional and nanostructured thermal barrier coatings on the GH2132 alloy were investigated.

2. Experimental materials and procedures

2.1. Materials and coating preparation

Thermal barrier coatings, composed of a bond coating and a top coating, were air-plasma-sprayed on a GH2132 alloy (Fe–25Ni–15Cr) substrate. The substrate geometry was a square of 20×20 mm^2 surface area with 3 mm thickness. The spraying material for the bond coat was microstructured NiCoCrAlY and the top coat was nanostructured and microstructured yttria stabilized zirconia (YSZ, ZrO_2–8 wt.% Y_2O_3). The chemical composition and original particle size of bond coat and top coat are shown in Table 1. Because of the poor flow ability of the original nanostructured YSZ that was unsuitable for plasma spraying, the original nanostructured YSZ were agglomerated before spraying. Firstly, a water-soluble binder of 4% polyvinyl alcohol (PVA) in volume fraction in water at 95 °C was prepared. After cooling to room temperature, an organic binder of PVA was prepared. Then, the nanostructured YSZ and the organic blinder of PVA were evenly mixed by a stirrer. After the ultrasonic treatment, the mixtures were put into a drying box for heat treatment at 150 °C for 5 h. Finally, spherical agglomerated particles were obtained. The particles size in the range of 20–80 μm was chosen for plasma spraying. Prior to spraying process, the substrates were successively ground with SiC paper up to 800# (10 μm). They were then cleaned

* Corresponding author. Tel./fax: +86 451 86402345.
E-mail address: liyao@hit.edu.cn (Y. Li).

0257-8972/$ – see front matter © 2012 Elsevier B.V. All rights reserved.
http://dx.doi.org/10.1016/j.surfcoat.2012.11.074

Table 1
Chemical composition and particle size of materials.

Type of TBC		YSZ	NiCoCrAlY
Nanostructured	Layer thickness	250 μm	110 μm
		40–50 nm (before agglomeration)	
	Particle size	20–80 μm (after agglomeration)	45–90 μm
Microstructured	Layer thickness	250 μm	110 μm
	Particle size	45–75 μm	45–90 μm

Note: Original nanostructured YSZ powders were supplied by Hefei Health Kun Chemical Co., Ltd., Anhui, China; original microstructured YSZ and NiCoCrAlY powders were supplied by Beijing General Research Institute of Metal Research Institute, Beijing, China.

by absolute ethyl alcohol in an ultrasonic set. Subsequently, the substrates were placed into the air plasma spray (APS) system (Switzerland PT Corporation, R-750C) for overlaying with NiCoCrAlY bond coating. The as-sprayed substrates were then grit blasted by alumina particles with the size of 125 μm. As the thermal expansion mismatch of YSZ, NiCoCrAlY and Fe-cased superalloy, the as-sprayed substrates were preheated at 95 °C for 5 min prior to the TBCs' spraying. Nanostructured and microstructured YSZ were sprayed onto as sprayed bond coat specimen by an APS system, respectively. The APS parameters for depositing nanostructured and microstructured TBCs are given in Table 2.

2.2. Thermal shock test

The thermal shock test was carried out in a muffle furnace. When the temperature of the furnace reached up to 900 °C, the specimens were pushed into the furnace. The specimens were held about 300 s in the furnace, and then they were directly quenched into the water. As the water for test was so capacious, the temperature raise of water was not obvious. After 60 s, the temperature of specimens was as same as water according to the test of a thermometer contacted the surface of specimens. The temperature of water throughout the cycling was between 25 and 37 °C. More than 50% of the cracked and spalled region of the surface of top coating was adapted as criteria for the failure of the coating, and three parallel tests were carried out for each condition. The water-quenched thermal shock test was also performed by other investigations [18,19].

2.3. Surface and cross-sectional morphology examination

The surface, cross-sectional morphologies were examined by SEM. A high resolution digital camera was also employed to observe the macrostructure of coatings before and after thermal shock tests. As well, X-ray diffraction was used to further examine the phase composition of coatings.

3. Results and discussions

3.1. Microstructure and component of as-sprayed coatings

Surface, cross-sectional morphologies and XRD patterns of as-sprayed nanostructured and microstructured TBCs are shown in Fig. 1. By comparison of the surface morphologies of both coatings, displayed in Fig. 1(a) and (b), obvious unmelted particles on the surface of microstructured TBCs are observed. Because of the shrinkage of melted particles after spraying to room temperature, surface microcracks are observed for both coatings. The cross-sectional morphologies of both as-sprayed coatings in Fig. 1(c) and (d) indicate that both coatings comprise a low-density top coat of YSZ, a bond coat and the metallic substrate. A lamellar structure made of mechanically interlocking molten splats and high micro-scaled porosities are the characteristics of both as-sprayed TBCs. And the low density of YSZ is due to the fact that during the spraying process particles of YSZ is not thoroughly melted which results in less plastic deformation upon collision which the bond coat surface [20]. The XRD patterns of both YSZ surfaces are shown in Fig. 1(e), in which very week peaks of monoclinic phase (m-ZrO_2) and strong peaks of nonequilibrium tetragonal phase (t′-ZrO_2) are shown. The formation of t′-ZrO_2 is depended on the content of Y_2O_3 and the cooling rate [21]. 8%Y_2O_3 used in the present work ensures the stabilization of ZrO_2 during cooling, and high cooling rate of water quench prohibits the cube phase (c-ZrO_2) transforming to equilibrium tetragonal phase (t-ZrO_2), consequently t′-ZrO_2 form.

Table 2
Processing parameters for spraying coatings.

Parameter	Nano-YSZ	Micro-YSZ	NiCoCrAlY
Current (A)	550	550	450
Voltage (V)	57.3	57.3	57.3
Primary gas, Ar (l/min)	39	39	37
Secondary gas, H_2 (l/min)	7	8	2
Powder feed rate (g/min)	40	40	30
Spray distance (cm)	7	7	15

3.2. Surface crack evolution during thermal shock process

Considering the “edge effect” in the practical application of thermal barrier coatings, such as edges and corners in combustor and blade rim, square specimens were used. The previous investigation on the specimen geometry effect on the thermal shock behavior indicated that square specimens showed different thermal shock behavior [22].On the edge and corner of square specimens, spallation and delamination failures occurred. Additionally, bending and distortion of substrate were observed.

The surface crack evolution for both coatings during thermal shock is shown in Fig. 2. It can be seen that cracks initially occur at the corner of the specimens due to the extreme heating and cooling conditions encountered at the edges and then annularly propagate to the adjacent areas on further cycling. In the case of microstructured TBCs shown in Fig. 2(a), the first cracked failures initiated from the corner of the specimen at 30 cycles of testing, and severely cracks and local spallation appeared at 60 cycles. For nanostructured TBCs, the first cracked failures occurred at 50 cycles, and severely cracks and local spallation emerged at 150 cycles, as displayed in Fig. 2(b). In addition, distortion at edges occurs when the macrocracks indeed form at edges. And the distortion is more and more severe when the thermal cycling is increased, which is a typical characteristic for square specimens during thermal shock [19,22–24].

3.3. Failure of thermal barrier coatings by thermal shock

Thermal shock resistance is depended on the size and distribution of pores or existing cracks in coating. Thermal cycling can result in the cracking and spalling of TBC. It is due to the fact that cyclic thermal loads can cause horizontal or vertical cracks to propagate resulting in delamination/spallation of the coating and loss of thermal protection to the substrate [25].

Cross-sectional morphologies reveal the failure of thermal barrier coatings, and further verify the thermal shock resistance. Fig. 3 shows the cross-sectional morphologies of microstructured TBCs after 30-cycle, 50-cycle and 60-cycle thermal shock tests, respectively. After the thermal shock tests, four types of cracks were formed in the TBCs, i.e., vertical crack, horizontal crack, propagating crack, and one kind of special crack. The special crack that vertical cracks penetrate the bond coat to the substrate surface is defined as penetrating crack. At 30 cycles, vertical cracks and propagating crack (or horizontal crack) emerged in top coat. Penetrating crack was also observed. Reaching to 50 cycles, penetrating cracks became the main type of cracks. Short horizontal cracks emerged in top coat. Discontinuous oxide formed at the bond coat and substrate interface beneath the penetrating crack. Up to 60 cycles, spallation was observed on the surface of TBCs. Continuous oxide layer was shown at

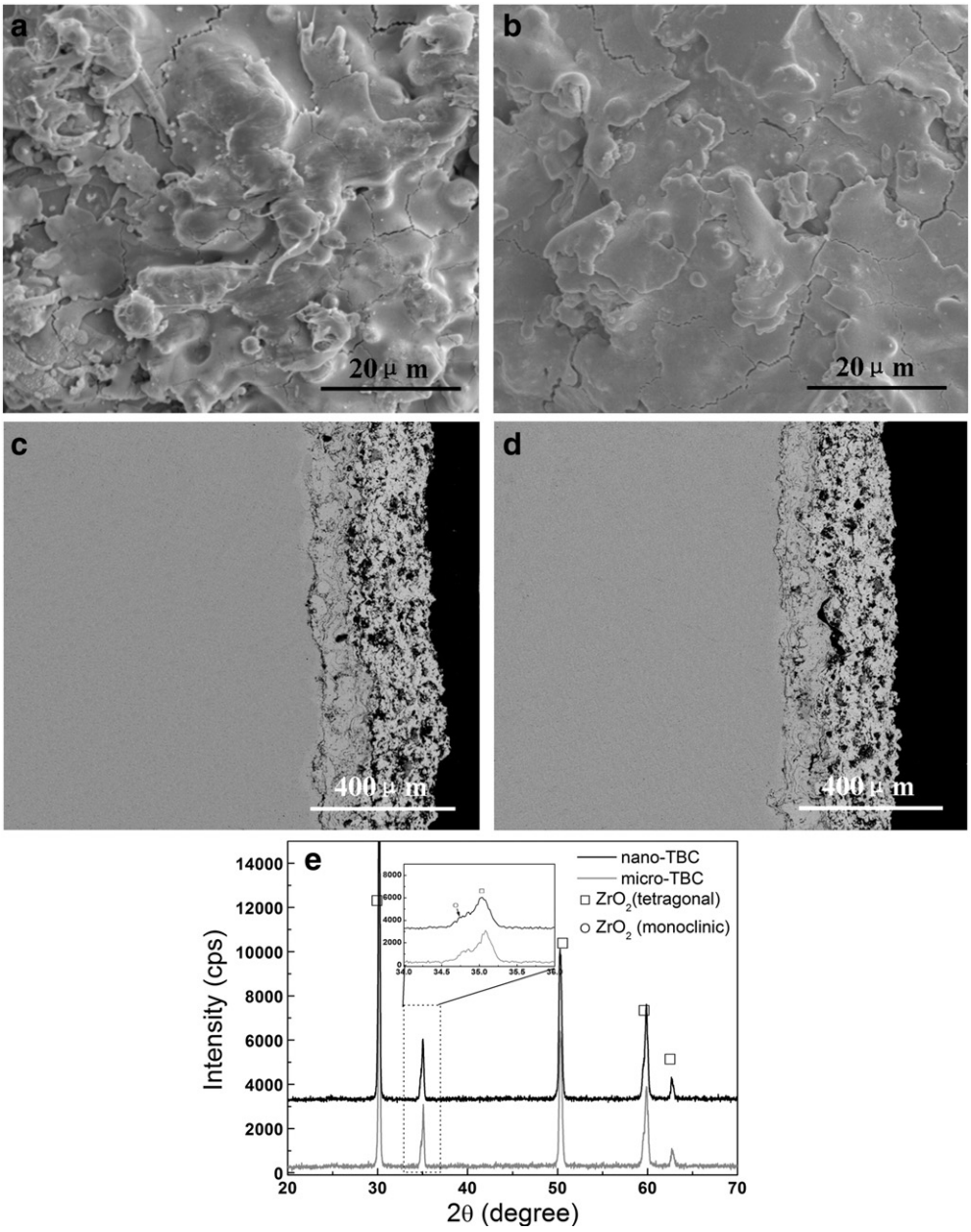

Fig. 1. The surface, cross-sectional morphologies of as-sprayed (a and c) microstructured and (b and d) nanostructured TBCs, and (e) the phase compositions.

the bond coat and substrate interface. The bond coat and the TBC separated from the substrate. In addition, horizontal cracks passed through the top coat.

For nanostructured TBCs, the cross-sectional morphology only showed vertical crack at 50-cycle thermal shock test. Until 60 cycles, penetrating crack occurred. However, no obvious oxide generated at the bond coat and the substrate interface, which is different with microstructured TBCs. Up to 150 cycles, the penetrating crack widened and island oxide formed at the bond coat and the substrate interface beneath the penetrating crack. In addition, horizontal crack between two penetrating cracks passed through mostly the top coating.

3.4. Failure mechanisms for nanostructured and microstructured thermal barrier coatings by thermal shock

Previous studies showed that the major factors causing failure of TBCs were TGO growth and thermal stresses [26,27]. In the thermal shock tests with a short heating time for each cycle, failure of TBCs was due to the thermal stress [27]. This was verified by observing the cross-sectional SEM images in Figs. 3 and 4. Though both the TBCs failure after 60-cycle and 150-cycle tests, respectively, no oxide form at the top coat and bond coat interface. Until the vertical crack penetrates the bond coat, as shown in Figs. 3(b) and 4(c), oxide form at the bond coat and substrate interface. Then those oxides might become the cause of TBCs failure. Therefore, the thermal stress is the virtual reason for the TBCs failure.

During the thermal shock test, the plane tensile stresses were increased with increase in the cycling number because of the thermal expansion difference between the coatings and substrate [3]. At cooling stage, the top coat is compressive and prone to induce the short horizontal cracks [28]. Increasing the cycles, the horizontal cracks would be linked to pass through mostly the top coat, and therefore the top coat will spall. However, the thermal expansion coefficient of GH2132 is so higher than the bond coat and the top coat that the thermal stress can result in the vertical cracks firstly occurring rather than horizontal cracks during heating stage. The horizontal cracks in the top coat emerged after

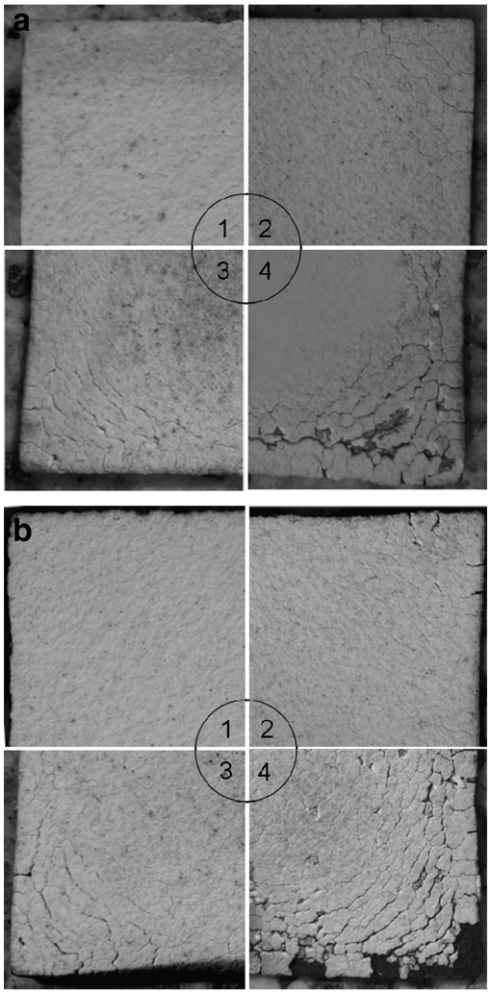

Fig. 2. Cracks evolution after thermal shock tests (a) microstructured YSZ; (b) nanostructured YSZ (a_1) 10 cycles; (a_2) 30 cycles; (a_3) 50 cycles; (a_4) 60 cycles; (b_1) 10 cycles; (b_2) 50 cycles; (b_3) 60 cycles; (b_4) 150 cycles.

more cycles at cooling stage. The vertical cracks easily penetrate through bond coat, and further expand to the bond coat and substrate interface where oxidation process occurs, as aforementioned results in Figs. 3 and 4. The brittle oxide formed at bond coat and substrate interface is the main causing of TBCs failure. This whole process is different from Ni-based alloy. In Ni-based alloy system, the oxidation initially occurs on the surface of bond coat. The failure is attributed to the TGO growth or Ni, Cr oxide formation [2,3,29,30].

The thermal expansion mismatch stress, using a balanced biaxial stress state approximation, is performed according to the following equation [31]:

$$\sigma_{\Delta T} = \Delta T \cdot \Delta\alpha \cdot \frac{E}{1-\mu} \tag{1}$$

where ΔT is the temperature difference between the temperature after cooling and experimental temperature, $\Delta\alpha$ is the thermal expansion coefficient difference between ceramic coating and metallic substrate, E is the Young's modulus of ceramic coating, and μ is the Poisson's rate of ceramic coating. The thermal expansion mismatch stress was calculated according to the data of Ref. [32], as shown in Table 3. By comparing the calculated $\sigma_{\Delta T}$ in Table 3, the thermal expansion mismatch stresses of GH2132 from each temperature to room temperature are all higher than Ni-alloy. Such high stresses can induce the formation of cracks in top coat at heating stage, especially at the corner of square specimens where heating rate is faster than the center. The thermal expansion

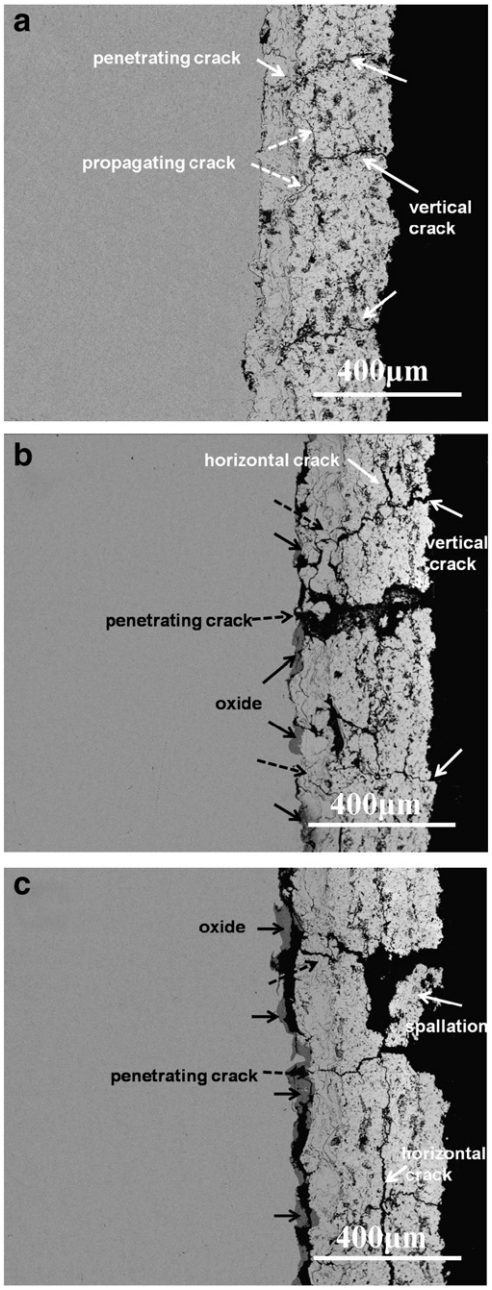

Fig. 3. The cross-sectional morphologies of microstructured TBCs after (a) 30-cycle, (b) 50-cycle, (c) 60-cycle thermal shock tests.

distortion of specimen at corner or edges is another reason of crack formation. Therefore, the initiated crack occurred at the corner of specimens. As the thermal expansion difference between the bond coat of NiCoCrAlY ($13.6–17.6\times10^{-6}$/°C, from 20 to 1100 °C, in Ref. [32]) and the GH2132 alloy is greater than the difference between TBC and GH2132, penetrating cracks occurred in bond coat was inevitable after the formation of vertical stress in top coat.

The different failures of microstructured and nanostructured TBCs are attributed to the different microstructures themselves. The effects of strain tolerance on the stress of TBCs can be seen more clearly by an analysis of the stress–strain curve of ceramic coatings [33], and the stress–strain curve for the TBCs was nonlinear and could be expressed by Shi et al. [34]:

$$\varepsilon = \varepsilon^{e} + \varepsilon^{ne} \tag{2}$$

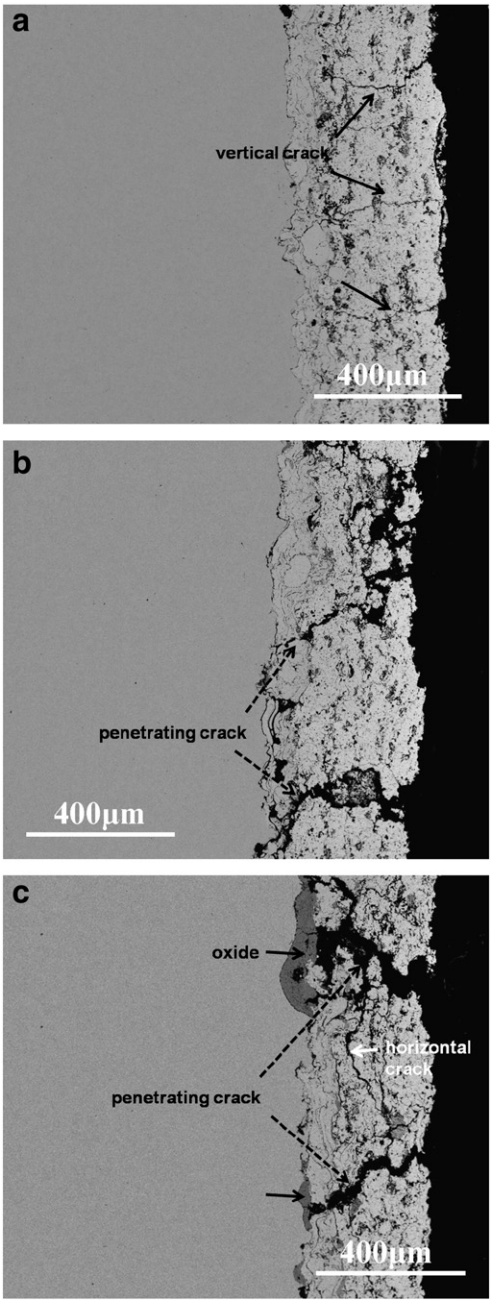

Fig. 4. The cross-sectional morphologies of nanostructured TBCs after (a) 50-cycle, (b) 60-cycle, (c) 150-cycle thermal shock tests.

Table 3
Mechanical chemical parameters of TBCs.

Temperature (T, °C)	Thermal expansion coefficient (α, $\times 10^{-6}$/°C)			Poisson's ratio (μ)	Young's modulus (E, GPa)	$\sigma_{\Delta T}$ (GPa)	
	TBC	Ni-alloy	GH2132 [a]			Ni-alloy	GH2132
400	9.6	15.6	16.8	0.10	44	−0.11	−0.13
600	10.1	16.2	17.5	0.11	40	−0.16	−0.19
800	10.8	16.9	19.1	0.11	34	−0.18	−0.25
1000	11.7	17.5	19.7	0.12	26	−0.17	−0.23
1100	12.2	18.0	20.45	0.12	22	−0.16	−0.22

[a] The thermal expansion coefficient of GH2132 was supplied by supplier, and other mechanical chemical parameters were cited from Ref. [32], the cooling temperature to room temperature of 25 °C.

where ε^e represents

$$\varepsilon^e = \frac{\sigma}{E} \tag{3}$$

which is the nominal strain and is estimated on the basis of linear elastic behavior, and where ε^{ne} represents the inelastic strain resulting from laminar and microcrack structures. Both coatings in the present work are the same in the thickness of each layer, and the materials of TBCs are also the same. Then the change in fracture strain could be expected from the inelastic strain [34]. As the microcracks and defects in nanostructured ceramic coating is less than microstructured ceramic coating, nanostructured ceramic coating is advantage for increasing the strain tolerance of the top coat. And the total strain ε of the top coat increase. Therefore, nanostructured ceramic coatings enhanced the durability of TBCs in thermal shock behavior. Moreover, large numbers of grain boundaries exist in the nanostructured ceramic coating, which can release most stress in the form of grain boundary slip rather than brittle fracture [16,35]. This not only delays the formation of vertical crack, but also limits the number of vertical cracks. Nevertheless, the penetrating cracks are inevitable occurred due to the greater thermal expansion mismatch difference between bond coat and substrate. Oxygen is easier to transport along these penetrating cracks to the substrate surface where oxidation occurs, and the oxidation expands along the bond coat and substrate interface to form local oxidation zone. In the case of microstructured TBCs, oxidation zone easily linked to form oxidation layer because the density of penetrating cracks is higher. Further increasing the cycles, the segmentation cracks pass through the oxide because of its brittlement. Finally, the bond coat and TBC are separated from substrate, as shown in Fig. 3(c). Owing to the low density of vertical crack for nanostructured TBCs, the oxidation zone is located at the place of penetrating cracks. Until 150 cycles, the penetrating cracks only widened and local horizontal cracks pass through the top coat between two penetrating cracks, as shown in Fig. 4(c). As a whole, microstructured TBCs absolutely lose the function of protection and heat insulation after 60-cycle thermal shock test. Nanostructured TBCs still can play a role in heat insulation after 150 cycles though spallation occurred at the edge and corner to square specimens.

4. Conclusions

The thermal shock tests of nanostructured and microstructured thermal barrier coatings on the GH2132 alloy were investigated in a comparative aspect. The major conclusions are as follows:

(1) In all cases, the initially cracks generated at the corner of the square specimen.
(2) A continuous oxide layer formed at the interface of bond coat and substrate, which resulted in the failure of microstructured thermal barrier coatings.
(3) Attributing to the nanocrystallization, the nanostructured thermal barrier coatings displayed better thermal shock resistance.

Acknowledgments

This work was supported by National Natural Science Foundation of China (nos. 51010005 and 90916020) and the Program for New Century Excellent Talents in University (NCET-08-0168).

References

[1] R.A. Miller, Surf. Coat. Technol. 30 (1987) 1.
[2] N.P. Padture, M. Gell, E.H. Jordan, Science 296 (2002) 280.
[3] A.G. Evans, D.R. Mumm, J.W. Hutchinson, G.H. Meier, F.S. Pettit, Prog. Mater. Sci. 46 (2001) 505.
[4] X.Q. Cao, R. Vassen, D. Stoever, J. Eur. Ceram. Soc. 24 (2004) 1.
[5] C.G. Levi, Curr. Opin. Solid State Mater. Sci. 8 (2004) 77.
[6] R.L. Jones, J. Therm. Spray Technol. 6 (1997) 77.
[7] S.R. Choi, D.M. Zhu, R.A. Miller, Int. J. Appl. Ceram. Technol. 1 (2004) 330.

[8] S. Hayashi, W. Wang, D.J. Sordelet, B. Greeson, Metall. Mater. Trans. A 36 (2005) 1769.
[9] D. Zhu, R.A. Miller, Surf. Coat. Technol. 108–109 (1998) 114.
[10] R. Vaßen, N. Czech, W. Mallener, W. Stamm, D. Stöver, Surf. Coat. Technol. 141 (2001) 135.
[11] B. Siebert, C. Funke, R. Vaßen, D. Stöver, J. Mater. Process. Technol. 92–93 (1999) 217.
[12] Y.H. Zhang, P.J. Withers, M.D. Fox, D.M. Knowles, Mater. Sci. Technol. 15 (1999) 1031.
[13] E. Tzimas, H. Müllejans, S.D. Peteves, J. Bressers, W. Stamm, Acta Mater. 48 (2000) 4699.
[14] B. Baufeld, E. Tzimas, P. Hähner, H. Müllejans, M.P. Peteves, Scr. Mater. 45 (2001) 859.
[15] B. Liang, C.X. Ding, H.L. Liao, C. Coddet, Surf. Coat. Technol. 200 (2006) 4549.
[16] B. Liang, C.X. Ding, Surf. Coat. Technol. 197 (2005) 185.
[17] R.S. Lima, A. Kucuk, C.C. Berndt, Surf. Coat. Technol. 135 (2001) 166.
[18] A.N. Khan, J. Lu, Surf. Coat. Technol. 201 (2007) 4653.
[19] G. Di Girolamo, F. Marra, C. Blasi, E. Serra, T. Valente, Ceram. Int. 37 (2011) 2711.
[20] B. Saeedi, A. Sabour, A.M. Khoddami, Mater. Corros. 60 (2009) 695.
[21] X.H. Xiang, J.C. Zhu, Z.D. Yin, Z.H. Lai, Surf. Coat. Technol. 88 (1996) 66.
[22] E. Altuncu, E.I. Karaall, G. Erdogan, F. Ustel, A. Turk, Plasma Process. Polym. s6 (2009) 711.
[23] J. Wu, H. Guo, L. Zhou, L. Wang, S.K. Gong, J. Therm. Spray Technol. 19 (2010) 1186.
[24] A.P. Raheleh, S.R. Reza, M. Reza, J. Hossein, Opt. Lasers Eng. 50 (2012) 780.
[25] K. Kokini, J. DeJong, S. Rangaraj, B. Beardsley, Surf. Coat. Technol. 154 (2002) 223.
[26] K.A. Nusair, J. Lu, Surf. Coat. Technol. 201 (2007) 5143.
[27] S. Ahmaniemi, P. Vuoristo, T. Mantyla, C. Gualco, A. Bonadei, R. Di Maggio, Metall. Trans A 36 (2005) 1841.
[28] C.H. Hsueh, J. Appl. Phys. 91 (2002) 9652.
[29] B. Gleeson, J. Propuls. Power 22 (2006) 375.
[30] H. Echsler, V. Shemet, M. Schütze, L. Singheiser, W.J. Quadakkers, J. Mater. Sci. 41 (2006) 1047.
[31] R.A. Miller, C.E. Lowell, Thin Solid Films 95 (1982) 265.
[32] Y.C. Zhou, T. Hashida, Int. J. Solids Struct. 38 (2001) 4235.
[33] H.L. Tsai, P.C. Tsai, J. Mater. Eng. Perform. 4 (1995) 689.
[34] K.S. Shi, Z.Y. Qian, M.S. Zhuang, J. Am. Ceram. Soc. 71 (1988) 924.
[35] X.L. Jiang, C.B. Liu, F. Lin, J. Mater. Sci. Technol. 23 (2007) 449.